Nucleolar stress triggers the irreversible cell cycle slow down leading to cell death during replicative aging in *Saccharomyces cerevisiae*

Sandrine Morlot[1234], Song Jia[1234], Isabelle Léger-Silvestre[5], Audrey Matifas[1234], Olivier Gadal[5], Gilles Charvin[1234].

[1]Developmental Biology and Stem Cells Department, Institut de Génétique et de Biologie Moléculaire et Cellulaire, Strasbourg, France;

[2]Centre National de la Recherche Scientifique, Illkirch, France;

[3]Institut National de la Santé et de la Recherche Médicale, Illkirch, France;

[4]Université de Strasbourg, Illkirch, France;

[5]Laboratoire de Biologie Moléculaire Eucaryote, Centre de Biologie Intégrative (CBI), Université de Toulouse, CNRS, UPS, Toulouse 31000, France;

Abstract

Asymmetric division in *Saccharomyces cerevisiae* generates an aging mother cell and a rejuvenated daughter cell. The accumulation of Extrachromosomal rDNA Circles (ERCs) and their specific retention in mothers have been hypothesized to be responsible for replicative aging. However, it remains unclear by which molecular mechanisms ERCs would trigger the cell cycle slow-down occurring during replicative aging and leading to cell death. In this study, we show that ERCs accumulation is initiated within the 5 divisions preceding the onset of cell cycle decline. The generation of ERCs is also concomitant with a nucleolar stress characterized by an up-regulation of RNA polymerase I activity and an accumulation of pre-rRNAs in the nucleolus which do not lead neither to a higher production of ribosomes, nor to an increased growth rate. We further demonstrate that this nucleolar stress observed in old mothers is not inherited by daughters, which recover basal RNA polymerase I activity and normal cell cycle durations following an asymmetrical nuclear division. In the long-lived mutant *fob1Δ*, we identified a sub-population, with a further extended longevity, which does not present neither a nucleolar stress nor a cell cycle slow down prior to cell death. Altogether, these findings support a causal role for the nucleolar stress in entering cellular senescence.

Introduction

Budding yeast cells undergo a limited number of asymmetrical divisions before entering senescence and eventually dying, a phenomenon known as replicative aging (Mortimer and Johnston, 1959). Unlike symmetrically dividing unicellular organisms (Nakaoka and

Wakamoto, 2017; Spivey et al., 2017), the replicative lifespan (RLS) in budding yeast follows a broad Gaussian distribution within a population, indicating that cell death is not a stochastic process, yet presents large cell-to-cell variability. Importantly, while the replicative age of mothers increases at each division, new born daughter cells recover a full replicative potential (Kennedy et al., 1994). Such rejuvenation of daughter cells led to postulate that cell death results from the accumulation of aging factors in mothers, which are asymmetrically segregated upon cell division (Egilmez and Jazwinski, 1989).

The accumulation of Extrachromosomal ribosomal DNA Circles (ERCs) in aging mothers was the first potential aging factor that was studied in detail (Sinclair and Guarente, 1997). ERCs result from the excision of repeats from the rDNA cluster located on chromosome XII. This genomic region contains the highly transcribed 35S ribosomal RNA genes in tandem repeats (approximately 150 copies). A replication fork barrier (RFB), where the protein Fob1 binds, prevents the collision between the replication fork and the RNA polymerase I transcription of 35S rRNA gene (Brewer and Fangman, 1988; Kobayashi, 2003). The repetitive nature of the rDNA cluster and the stalling of the DNA replication complex at the RFB, which favors double strand breaks, promote recombination events. ERCs were shown to progressively accumulate in aging cells due to the presence of an autonomously replicating sequence (ARS) on each rDNA repeat, that ensures the amplification of the excised DNA circles over successive divisions (Sinclair and Guarente, 1997). Strains deleted for the *FOB1* gene present lower amount of ERCs and an extended lifespan (Defossez et al., 1999) which further correlates accumulation of ERCs with replicative aging. Finally, to explain daughter rejuvenation with the ERC accumulation model, it was proposed that a diffusion barrier at the bud neck prevents the ERCs from being inherited by the daughter cells during cell division (Denoth-Lippuner et al., 2014; Shcheprova et al., 2008).

However, maintaining low ERC levels by genetically decreasing the recombination probability at the rDNA locus is not enough to promote longevity (Ganley et al., 2009). Furthermore, it is not clear why ERC accumulation is toxic to the cell and how it would lead to an arrest of proliferation (Ganley and Kobayashi, 2014). Another hypothesis favors rDNA instability, in particular the activity of the non-coding bidirectional promoter, called Epro, which is responsible for the amplification of rDNA repeats, rather than ERCs accumulation as being

involved in replicative aging (Kobayashi, 2008; Saka et al., 2013). Hence, the mechanism that links rDNA regulation and replicative aging remains to be elucidated.

The dynamics of aging in budding yeast has been previously characterized by an abrupt transition, called the Senescence Entry Point (SEP), between an healthy state with regular and robust divisions and a senescent-like state where cell cycles are much longer and variable (Fehrmann et al., 2013). The molecular pathways responsible for this abrupt cellular transition are still not understood. In particular, it is not known how ERCs, rDNA instability and nucleolar activity, good candidates for aging factors, are linked to the SEP.

In this study, we analyzed in vivo the aging process in single yeast cells over multiple generations using microfluidic tools and videomicroscopy. We show that a dramatic nucleolar stress combined with the accumulation of ERCs precede the SEP. This nucleolar stress is characterized by an upregulation of rDNA transcription and an accumulation of pre-rRNAs in the nucleolus followed, by an enlargement of the nucleus concomitantly with the irreversible cell cycle slow down. Altogether, these findings highlight that the nucleolar steps of ribosome biogenesis play a critical role in the aging process.

Results

The number of rDNA repeats and the nucleolar volume increase before the irreversible cell cycle slow down leading to cell death

To follow the real-time dynamics of the rDNA cluster during replicative aging in individual yeast cells, we used a previously developed strain (Miyazaki and Kobayashi, 2011), in which LacO sequences are inserted in all repeats of the rDNA array (Fig1A). Thus, by monitoring LacI-GFP signal within the nucleolus delimited by NET1-mCherry fluorescence, we could estimate the evolution of rDNA repeats number in single mother cells trapped from birth to death in a microfluidic device (Fig1A) (Goulev et al., 2017). The senescence entry point (SEP) is a particularly critical time point in yeast lifespan as it corresponds to the abrupt cell cycle slow down occurring before cell death (Fig1B and 1C) (Fehrmann et al., 2013). We thus analyzed fluorescence signals after SEP alignment rather than birth alignment which smoothens the cell cycle dynamics. We observed that the total GFP-LacI fluorescence within the nucleolus increased significantly by 60% within the 5 divisions preceding SEP and further increased to 4.4-fold 5 divisions after SEP (Fig1D). If considering 150 repeats as the basal size of the rDNA

cluster, fluorescence measurements allow us to estimate an increase to 240 repeats before SEP and to more than 600 repeats after SEP. Therefore, this increase is likely to originate from ERCs accumulation as wild type cells hardly accumulate more than 200 repeats within the rDNA cluster (Ide et al., 2013). In agreement with this result, we also found an increased signal of FOB1-GFP before SEP (FigS1A), which suggests a higher rate of blocked replication forks at RFB before SEP and thus a higher rate of ERCs production. Interestingly, NET1-mcherry signal increased to a larger extent than GFP-LacI before (3.9-fold) and after SEP (25-fold) (Fig1D and FigS1D). The nucleolar size has been shown to correlate positively with the cellular volume (Jorgensen et al., 2007). However the sudden increase in NET1-mCherry signal was not due to an abrupt cell size enlargement as the cell area maintained a constant dynamics during the SEP transition (FigS1B). This increase of NET1-mCherry fluorescence was mainly due to an enlargement of the nucleolar volume as NET1-mCherry mean fluorescence increases only by 36% after SEP (FigS1D) which was much lower than the 17-fold increase of the segmented area (FigS1C).

These results highlight that the nucleolus undergoes two major modifications prior to cellular senescence: increased copy number of ribosomal RNA genes and volume expansion.

rDNA transcription and rRNAs processing are up-regulated before SEP

We found a dramatic increase in the nucleolar volume occurring before the SEP. The nucleolus is the nuclear region were pre-rRNAs are synthetized and processed. Therefore we investigated the dynamics of rDNA transcription and pre-rRNAs levels during the SEP transition.

We first monitored the total amount of RNA Pol1 by following its largest subunit RPA190, fused to GFP, throughout yeast lifespan (Fig2A). We measured an increase by 70% in RPA190-GFP total fluorescence over the 5 divisions preceding SEP, followed by a larger increase (up to 7-fold) after SEP (Fig2B). To establish if this increased level of RNA Pol1 led to higher transcription at the rDNA locus, we measured the amount of pre-rRNAs in the nucleolus by performing RNA FISH on aging cells directly in the microfluidic chip (“FiSH on Chip”). We stopped the time-lapse experiment after 60 hours acquisition, when the microfluidic device was fully loaded and the ages of trapped mother cells were spread before and after SEP, as cells growing in cavities were not synchronized (left graphs Fig2C and 2D). We then performed

RNA FISH staining on chip after cell fixation and cell wall digestion. The FISH probe targeted specifically the ITS1 region so that all pre-rRNAS from 35S to 20S would be labelled. FISH staining and RPA190-GFP signal presented a good colocalization, as expected (right panels in Fig2C and 2D). For cells in a pre-SEP state (constant and short division timings), we measured a strong positive correlation (black dots in Fig2C, Pearson corr. coef. = 0.8) between the fluorescence levels of FISH probes and RPA190-GFP, indicating that the amount of pre-rRNAs scaled with the amount of RNA Pol1. For cells having already experienced SEP before fixation and FISH staining, the positive correlation remained even though to a lower extent (magenta stars in Fig2C, Pearson corr. coef. = 0.5) (Fig2C), suggesting that the amount of RNA Pol1 and the rate of transcription could be uncoupled in senescence. We measured a 4.4-fold increased amount of RNA Pol1 and a 2.6-fold increase of pre-rRNAs after the SEP transition (boxplot Fig2C). These results show that pre-rRNAs accumulate upon SEP in the nucleolus, but to a lower extent than RNA Pol1.

As RNA Pol1 showed an increasing amount before SEP (Fig. 2A), we tested whether pre-rRNAs levels followed a similar trend. To address this question, we focused on pre-SEP cells (black dots on Figure 2C) and compared “early pre-SEP” cells (blue diamonds in Fig2D) having experienced less than 5 divisions with “late pre-SEP” cells (green dots in Fig 2D) having undergone more than 10 divisions. Late pre-SEP cells are more likely than early pre-SEP cells to be close to the SEP and thus to present a higher level of RPA190-GFP. Indeed, we measured a 3.8-fold increase of RPA-GFP fluorescence in the late pre-SEP cells (boxplot Fig2D). We observed a good correlation between RNA Pol1 amount and FISH fluorescence in the 2 subgroups (Pearson corr. coeff. = 0.8 for early pre-SEP and 0.7 for late pre-SEP, Figure 2D). Moreover, we measured a 3.9-fold increase in the pre-rRNAs levels in the late pre-SEP cells, similar to the 3.8-fold increase in Pol1 levels (Fig2D). These results show that pre-rRNAs levels follow a dynamics very similar to RNA Pol1 before SEP. We thus conclude that there is an accumulation of pre-rRNAs in the nucleolus before the entry into senescence. To further validate the nucleolar accumulation of pre-rRNAs before SEP, we also performed RNA FISH in aging cells containing the NET1-GFP marker (FigS2A), following the same procedure as described above. We found the same results as with RPA-190-GFP (higher levels of pre-rRNAs in post-SEP and late-pre-SEP cells), albeit with a lower correlation, as NET1 function is not directly linked to pre-rRNAs synthesis (FigS2B).

As the RNA FISH experiment could not discriminate between the successive transient pre-rRNAS from 35S to 20S, we could only state that transcription of rDNA was upregulated before SEP, but not necessarily rRNA processing. To test this latter hypothesis, we monitored SSF1 protein fused to GFP throughout aging (Fig2E). SSF1 is a component of the 66S pre-ribosomal particles, thus SSF1-GFP fluorescence is a good proxy for the nucleolar late steps of rRNA processing. Similarly to RPA190-GFP, we observed that SSF1-GFP fluorescence increased by 4.2-fold before and up to 24-fold after SEP (Fig2E). These results suggest that both co- and post-transcriptional processing of rRNAs are upregulated during the 5 divisions before SEP, and therefore constitute a novel hallmark of senescent cells.

The up-regulation of pre-rRNAs synthesis does not lead neither to an increase in ribosomes levels nor to a higher growth rate

We next wondered if the upregulation of nucleolar steps of ribosome biogenesis would lead to a higher production of ribosomes that would in turn increase the growth rate.

We first investigated if the nucleoplasmic processing of pre-rRNAs was up-regulated in a similar way as the nucleolar processing. By monitoring the protein NOG2, required for late pre60S maturation, fused to GFP (Fig3A), we could evaluate if the nuclear export of pre-RNAs was following the same dynamics as the previous steps of ribosome biogenesis. We measured a good scaling of NOG2-GFP levels with the cell area before SEP (Fig3B and FigS3A), in sharp contrast with the levels of RPA190-GFP and SSF1-GFP, which increased much faster than cell area from 5 divisions before SEP (Fig3G, 3H, S3D and S3E). Hence, our results highlight an uncoupling between the constant basal rate of nucleoplasmic maturation of pre-ribosomes and the upregulation of the nucleolar steps of ribosome biogenesis.

Next, we investigated whether the cytoplasmic level of ribosomes was modified during the SEP transition by following RPL13A, a component of the 60S ribosomal subunit, fused to GFP (Fig3C). Similarly to NOG2-GFP, we observed a constant ratio of RPL13A-GFP over the cellular area before SEP (Fig3D and FigS3B), indicating that the cytoplasmic concentration of ribosomes remained constant during the SEP transition while the ribosome biogenesis was activated in the nucleolus.

Finally, we estimated the growth rate based on the segmented contours in phase contrast of mother and daughter cells (Fig3E). In healthy cells, the activation of ribosome biogenesis in

the nucleolus normally responds to a higher demand in growth. In contrast, in aging cells experiencing a nucleolar expansion, we observed a constant growth rate until the SEP (Fig3F and FigS3C) in agreement with the constant concentration of ribosomes. Strikingly the growth rate started to significantly decrease at the SEP (Fig3F and FigS3C), while this dynamics is not noticeable for RPL13A-GFP and NOG2-GFP where a slight decrease occurred only several divisions after SEP (FigS3A and S3B). These results suggest that, in senescent cells, nucleolar ribosome biogenesis, cytosolic ribosome levels and growth rate could be uncoupled.

Altogether these results demonstrate that a nucleolar stress occurs within 5 divisions before the SEP. This nucleolar stress triggers the accumulation of pre-rRNAs in the nucleolus, which results in an extensive enlargement of the nucleolus compared to the cell volume (Fig3I).

The SEP is concomitant with a large increase in nucleoplasmic content.

As the nucleolar volume drastically increased before SEP, we looked at the dynamics of the whole nucleus. We measured the nucleus size with the nuclear reporter HTB2-sfGFP (Fig3J). We observed an abrupt increase in nuclear content, concomitantly with the SEP (Fig4D). This increase resulted in a striking loss of the nuclear to cellular volume ratio or N/C ratio (Fig3K and 4E). Importantly, this behavior is not specific to histones, as we observed the same dynamics with the nuclear reporter NLS-sfGFP under the control of *ACT1* promoter (FigS3F). Using the NLS-sfGFP reporter, the increase in N/C ratio occurred slightly before the SEP. We explain this difference by the fact that, with the NLS-sfGFP reporter, we followed the whole nucleus including the nucleolus, whereas with HTB2-sfGFP, we mainly measured the nucleoplasmic volume, as the nucleolus contains a low level of histones. Removing the NLS sequence abolished the sudden increase in sfGFP fluorescence at SEP (FigS3G), further highlighting the specific dynamics of the nucleus. The increase in N/C ratio is also peculiar when compared to the other organelles such as the vacuoles. Indeed using the vacuolar marker VPH1-GFP, we measured that the vacuole occupies a constant fraction of 30% of the cellular area throughout lifespan (FigS3H), while the nuclear area represents 10% of the cellular area before SEP and suddenly increases up to 40% after SEP (Fig3K, S3F, 4E). In addition, high N/C ratio is an atypical feature of aging cells as this ratio is known to be strongly robust in wild type young yeast cells and in numerous mutants including cell size and cell cycle mutants (Jorgensen et al., 2007; Neumann and Nurse, 2007).

Nucleolar stress is not transmitted to rejuvenated daughter cells

We have identified a nucleolar stress occurring in aging mother cells characterized by an upregulation, in the nucleolar steps, of ribosome biogenesis which is inefficient in producing more ribosomes and in increasing growth (Fig3L). According to the yeast replicative aging paradigm, aging markers are not transmitted to daughter cells, which recover a full replicative potential. To test if the nucleolar stress was consistent with daughter rejuvenation, we sought to determine whether daughters were born clear of the age-associated nucleolar markers.

To address this question, we took advantage of the cavities in our microfluidic device which allowed tracking successive daughters for a couple of divisions. Strikingly, we found that the daughter cells of post-SEP mothers recovered a short cell cycle duration (Fig4A). This revealed that substantial daughter rejuvenation occurred with one single division. As RNA Pol1 and pre-rRNAs were both shown to increase in mother cells prior to SEP, we measured the fluorescence of RPA190-GFP and SSF1-GFP markers in the successive daughters of aging mother cells. We noticed a constant basal amount of these proteins in daughters even when the levels increased in mothers (Fig4B and 4C). This demostrated that daughter cells recovered a basal rDNA transcription and rRNA processing even when the mother already acquired an up-regulated nucleolar activity.

In addition, as senescent mother cells present enlarged nuclei, we measured the nuclear size in daughter cell with HTB2-sfGFP fluorescence. We observed a constant level in daughters while the signal increased in mothers (Fig4D). The N/C ratio was also rescued in daughter cells (Fig4E), further illustrating that the nucleolar stress affecting aging mothers is not transmitted to rejuvenated daughters (Fig4F).

Altogether, these results demonstrate that the nucleolar stress is indeed an early aging marker accumulating specifically in mothers.

Nucleolar stress and cell cycle slow down are triggered by the same stochastic event

We have established that the nucleolar stress is an early aging marker, followed by an irreversible cell cycle slow down, and subsequent cell death. We then investigated if these two events (nucleolar stress and cell cycle slow down) were mechanistically connected, by looking at the aging dynamics in the long-lived strain fob1Δ. The mutant fob1Δ has been shown to present a lifespan extension of 30% compared to wild type (Defossez et al., 1999). In

agreement with the literature, we also measured an enhanced longevity for fob1Δ in our microfluidic device (Table 1, Fig5A). Interestingly, a large majority (68.3%) of fob1Δ cells do not present any cell cycle slow down before death while only 6.6% of WT cells have no SEP transition (Table1, Fig5B and 5C). These fob1Δ cells without SEP present a further increased lifespan (RLS=37, Fig5A) than the fob1Δ cells experiencing a SEP (RLS=34, still longer-lived than WT). In fob1Δ cells undergoing a SEP, the onset of cell cycle slow-down is delayed (Table1) but the dynamics of the cell cycle slow-down is similar to WT (Fig5D), suggesting that the same mechanisms drive replicative aging in both populations. Thus, within a single isogenic strain aging in a well-controlled environment emerge two distinct sub-populations: the "fob1Δ NO SEP" population which keeps a constant and robust cell cycle until cell death and the "fob1Δ with SEP" population experiencing a delayed SEP. Hence, SEP is a stochastic process and the gene FOB1 influences the probability to undergo a SEP.

We took advantage of these two populations within the fob1Δ strain to better characterize the role of nucleolar stress in replicative aging. We analyzed the fluorescence of RPA190-GFP, subunit of RNA Pol1. The population "fob1Δ with SEP" experienced a significant increase of RPA190-GFP fluorescence before SEP similar to WT and cells died with a large amount of RNA Pol1 (Fig5F). In contrast, the "fob1Δ NO SEP" population kept a basal level of RPA190-GFP throughout lifespan (Fig5G) and cells died with a physiological level of RNA Pol1 even after more than 30 divisions (Fig5E). Daughter cells of both populations "fob1Δ NO SEP" and "fob1Δ with SEP" recover similar levels of RPA190-GFP (FigS4A), showing that the maintenance of small nucleoli in "fob1Δ NO SEP" is not due to a lower retention of aging factors in mothers but rather to a better maintenance of nucleolar activity during aging. Therefore "fob1Δ NO SEP" cells keep a constant nucleolar activity throughout lifespan whereas fob1Δ cells with a SEP experience an increase in nucleolar activity similar to WT.

We also measured the fluorescence of the nuclear marker HTB2-sfGFP in the two populations "fob1Δ NO SEP" and "fob1Δ with SEP". In agreement with the nucleolar dynamics, only the cells experiencing a SEP presented an increased level of HTB2-sfGFP very similar to WT (Fig5H). The 'fob1Δ NO SEP" population maintained a basal level of HTB2-sfGFP throughout lifespan and was able to maintain a typical N/C ratio around 0.1.

It is also worth noticing that WT, "fob1Δ with SEP" and "fob1Δ NO SEP" populations have similar cell area dynamics (FigS4B and S4C). When aligned from birth, cell area dynamics of

both fob1Δ populations overlap perfectly (FigS4B) suggesting that cell size control and SEP are not correlated. When aligned from SEP, fob1Δ cells present a slightly larger area than WT cells (FigS4C) showing that SEP is not triggered by a cellular volume threshold. These results reinforce the idea that cell size is not an aging factor. In conclusion, cells which are able to maintain a low nucleolar activity, keep a fast division rate and live longer. These results are in favor of a causal link between the nucleolar upregulation of ribosome biogenesis and the cell cycle slowdown characterizing senescence.

Discussion

By combining microfluidics, time-lapse microscopy and quantitative single cell analysis, we have uncovered that nucleolar stress is an early aging marker. Systematic comparison of relevant fluorescent reporters between aging mothers and rejuvenated daughters allowed us to identify the key players involved in replicative lifespan such as rDNA transcription and pre-rRNAs accumulation. The increased number of rRNA genes and the enhanced activity of RNA Pol1 are a unique feature of aging cells close to the senescence transition. Indeed, in healthy young yeast cells, only half of the 35S genes within the rDNA cluster are actively transcribed (Dammann et al., 1993) and RNA Pol1 activity is up-regulated, in a compensatory mechanism, only when the number of repeats in the rDNA cluster is reduced (Takeuchi et al., 2003). Furthermore, we were able to chronologically order the events leading to cell death. An upregulation of the initiation of ribosome biogenesis occurs in the nucleolus early during the cellular lifespan and is followed, within 5 divisions by a massive nuclear enlargement and the irreversible cell cycle slow-down, leading eventually to cell death (Fig3L and 4F). Finally, the analysis of long-lived mutants strongly suggest that the nucleolar stress triggers cellular senescence.

Ribosome biogenesis has been previously identified as a key pathway involved in yeast replicative aging in a genome-wide analysis of aged-sorted cell populations (Janssens et al., 2015). However, no mechanism connecting ribosome biogenesis and aging were described so far. Recently, it has also been shown that a sustained loss of silencing at the rDNA locus precedes cell death (Li et al., 2017). Our results show direct evidence of an unconventional activation of rDNA transcription leading to cellular senescence. This process is likely conserved across species as similar observations were also reported in several studies in metazoans. In the germline stem cells of Drosophila male, the rDNA array on chromosome X is silenced in

young flies but active in old flies (Lu et al., 2018). In mouse embryonic fibroblasts, oncogenic stress induces rRNA transcription and triggers cellular senescence (Nishimura et al., 2015). Our data precise that the transcription at the rDNA cluster is activated before the onset of cellular senescence in physiological conditions (no external induction of senescence). In particular, our work clearly demonstrates that nucleolar dysregulation is not a mere consequence of the aging process but appears before the establishment of a senescent state. More recently, it has been found that small nucleoli in post-mitotic cells are a hallmark of an extended longevity in *C. elegans*, Drosophila, Mice and human muscle tissues (Tiku et al., 2016). These results, together with our study, highlight the crucial role of the nucleolus in both replicative and chronological aging, suggesting the existence of a global and conserved nucleolar mechanism controlling longevity.

It still remains to be determined how nucleolar stress and nuclear enlargement affect growth and division leading to a senescent state. The loss of N/C ratio at SEP is a good candidate as the nuclear volume should normally robustly scale with the cellular volume (Neumann and Nurse, 2007). It has recently been shown that disrupting mRNA export machinery in *S. pombe* increases significantly the N/C ratio by accumulation of RNAs (Kume et al., 2017). In addition, premature rRNAs are known to be trapped within the nucleolus (Gadal et al., 2002). The transition from the nucleolus to the nucleoplasm is accompanied by major compositional changes in preribosome (Kressler et al., 2017). Thus the dramatic accumulation of pre-rRNAs trapped in the nucleolus could probably be directly responsible for the sudden loss of N/C ratio during replicative aging. This abrupt increase in nuclear volume might then trigger a pathway slowing down cell cycle to allow the cell to reach a volume matching its nuclear size. However, pre-ribosomal particles synthetized in senescent cells are not export-competent and remain in the nucleolus. Therefore growth rate does not increase, thus cellular volume never catches up the appropriate physiological N/C ratio, reinforcing the activation of the pathway slowing down cell cycle, which could explain the irreversibility of the senescent state. It will be challenging to test experimentally this hypothesis as age-related senescence is the only intervention to our knowledge which dramatically modifies the N/C ratio in budding yeast.

Finally we established that a stochastic event triggers nucleolar stress (and subsequently cellular senescence) almost systematically in WT cells and in a small fraction of fob1Δ cells. ERCs excision and/or rDNA cluster amplification are very likely to be this stochastic event. In

wild type cells, ERCs are generated by the FOB1-dependent stalling of the replication fork at RFB whereas in fob1Δ cells, ERCs are produced by the collision of the replication fork against RNA Pol1 transcription machinery. This latter event occurs less frequently than FOB1-dependent excision as only half of 35S genes are actively transcribed (Dammann et al., 1993) and less than one third of ARS are fired during S phase (Brewer and Fangman, 1988). Thus some fob1Δ cells would never experience any ERC excision event during their lifespan. This would explain the two sub-populations "fob1Δ NO SEP" and "fob1Δ with SEP" that we identified. We were not able to distinguish between ERCs accumulation and genomic rDNA amplification. However a recent study shows that ERCs, in young cells, actually constitute a reservoir of rDNA repeats which can reinsert in the genomic rDNA cluster in response to copy number loss (Mansisidor et al., 2018). Thus ERCs and genomic rDNA form together a dynamic steady state levels in healthy young cells which highly expands before senescence.

In conclusion, this study supports an aging model where ERC excision first triggers a nucleolar stress, which then causes a loss of nuclear homeostasis resulting in an irreversible decline in growth and division, both leading to cell death.

Figure legends

Figure 1: The number of rDNA repeats and the nucleolus size increase 5 divisions prior to SEP. (A) Top: sketch of LacO insertion on each rDNA repeat in a strain containing NET1-mCherry and GFP-LacI. Bottom: pictures of a mother cell, delimited by a yellow contour in the fluorescence channels, with GFP-LacI and NET1-mCherry markers, trapped in a cavity in a microfluidic device from birth to death. Scale bar: 5µm. (B) Left: duration of successive cell cycles for 3 single cells (magenta, cyan and orange). Middle: Average cell cycle duration as a function of age for single cell trajectories aligned from birth. (C) Left: same 3 single cells as in B aligned from SEP. Middle: Average cell cycle durations after SEP alignment. Right: normalized cell cycle duration for 4 classes of age: (1): more than 5 divisions before SEP, (2): 5 to 0 divisions before SEP, (3): 1 to 5 divisions after SEP and (4): more than 5 divisions after SEP; data are normalized to the average of the 1st class. (D) Total GFP-LacI fluorescence (arbitrary units) within the contour delimited by NET1-mCherry signal for the same 3 single cells as above (left) and averaged after SEP alignment (middle). Right: normalized GFP-LacI fluorescence for 4 classes of age. (E) Total NET1-mCherry fluorescence (arbitrary units) for the same 3 single cells as above (left) and averaged after SEP alignment (middle). Right: normalized NET1-mCherry fluorescence for 4 classes of age. N=49 mother cells (for all averaged curves).

Figure 2: rRNAs synthesis and processing are upregulated before SEP. (A) Mother cell with RPA190-GFP marker in a microfluidic chip. (B) Total RPA190-GFP fluorescence (arbitrary units) for 3 single cells (left) and averaged after SEP alignment (middle). Right: normalized RPA190-GFP fluorescence for 4 classes of age. N=61 cells. (C) and (D) FISH on CHIP. Left: examples of cell cycle trajectories and corresponding pictures of cells labeled by RNA FISH directly on the microfluidic chip after 60 hours time-lapse acquisition. Middle: RPA190-GFP fluorescence as a function of FISH probe fluorescence. Right: boxplot of relative fluorescence of RPA-190 and FISH probe for pre-SEP cells (N= 136 cells, black in C), post-SEP cells (N= 123 cells, magenta in C), early pre-SEP cells (N= 45 cells, blue in D) and late pre-SEP cells (N= 68 cells, green in D). (E) Left: mother cell with SSF1-GFP marker in a microfluidic chip. Middle: total SSF1-GFP fluorescence averaged after SEP alignment. Right: normalized SSF1-GFP fluorescence for 4 classes of age. N= 56 cells. Scale bar: 5µm (for all pictures).

Figure 3: Ribosome concentration and growth rate do not increase during the entry into senescence. (A) Mother cell with NOG2-GFP marker on a microfluidic chip before and after SEP. (B) Ratio of NOG2-GFP total fluorescence over cellular area as a function of generation, averaged after SEP alignment. N= 33 cells. (C) Mother cell with RPL13A-GFP marker on a microfluidic chip before and after SEP. (D) Ratio of RPL13A-GFP total fluorescence over cellular area as a function of generation, averaged after SEP alignment. N= 32 cells. (E) Sketch explaining the calculation of growth rate based on segmented contour of the mother cells before budding (light green), the mother cell at the end of the division (dark green) and the new born daughter (orange). (F) Growth rate (measured from projected area) as a function of generation, averaged after SEP alignment. N=36 cells. (G) Ratio of RPA190-GFP total fluorescence over cellular area as a function of generation averaged after SEP alignment. N= 61 cells. (H) Ratio of SSF1-GFP total fluorescence over cellular area as a function of generation averaged after SEP alignment. N= 56 cells. (I) Ratio of nucleolar area (based on NET1-GFP segmentation) over cellular area as a function of generation, averaged after SEP alignment. N= 44 cells. (J) Mother cell with HTB2-sfGFP marker on a microfluidic chip before and after SEP. (K) Ratio of nuclear area (based on HTB2-sfGFP segmentation) over cellular area (or N/C ratio) as a function of generation, averaged after SEP alignment. N= 42 cells. (L) Model: nucleolar stress precedes SEP during replicative aging. Scale bar: 5µm (for all pictures).

Figure 4: rRNA synthesis and nuclear size are rejuvenated to basal levels in daughter cells of aging mother. (A) Left: Cell cycle duration of mother (green) and daughter (orange) cells as a function of generation, averaged after SEP alignment. Right: normalized cell cycle duration of daughters (orange) and mothers (green) for 4 classes of mother age. N= 29 cells. (B) Left: picture of a senescent mother cell and its daughter cell with RPA190-GFP. Cell is delimited by a yellow contour and fluorescence signal by a red contour. Middle: RPA190-GFP total fluorescence in mothers (green) and daughters (orange) as a function of generation, averaged after SEP alignment. Right: RPA190-GFP normalized fluorescence in mother (green) and daughter (orange) cells for 4 classes of mother age. N= 21-61 cells. (C) Same as (B) for SSF1-GFP marker. N= 17-56 cells. (D) Same as (B) for HTB2-sfGFP marker. N=42 cells. (E) Left: N/C ratio of mother (green) and daughter (orange) cells as a function of generation, averaged after SEP alignment. Right: N/C ratio of daughters (orange) and mothers (green) for 4 classes of

mother age. N= 42 cells. (F) Model: daughter cells of senescent mother do not inherit nucleolar stress. Scale bar: 5µm (for all pictures).

Figure 5: Senescence entry point results from a stochastic process dysregulating nucleolar activity. (A) Survival curves of fob1Δ strain (N= 126) and WT (N= 61). (B) and (C) Cell cycle durations for 3 single cells of fob1Δ strain without any SEP before death (B) and with SEP (C). (D) Cell cycle duration averaged after SEP alignment for WT (green, N= 57) and fob1Δ cells with SEP (blue, N= 40). Fob1Δ cells without SEP (magenta, N= 84) were aligned from birth and generation 0 was set to 30 (median SEP for fob1Δ cells with SEP). (E) and (F): Pictures of fob1Δ cells with RPA190-GFP marker, just before death, without a SEP (E) and with a SEP (F). Cell is delimited by a yellow contour and fluorescence signal by a red contour. Scale bar: 5µm. (G) RPA190-GFP fluorescence and (H) HTB2-sfGFP fluorescence in WT (green), "fob1 with SEP" (blue), "fob1 NO SEP" (magenta) after SEP alignment. N= 20-61 cells.

Figure S1: related to Figure1. (A) Left: pictures of a mother cell with FOB1-GFP marker in a microfluidic chip. Middle: total FOB1-GFP fluorescence averaged after SEP alignment. Right: normalized FOB1-GFP fluorescence for 4 classes of age. N= 28 cells. Scale bar: 5µm. (B) Left: Cell area as a function of generation for 3 single cells (magenta, cyan, orange, same cells as in main Fig1) aligned from birth. Middle: Cell area for the same 3 single cells aligned from SEP. Right: Cell area as a function of generation, averaged after SEP alignment. (C) Left: segmented area of NET-mCherry signal for the same 3 single cells as above and main Fig1 aligned from SEP. Middle: averaged segmented area of NET1-mCherry after SEP alignment. Right: normalized NET1-mCherry segmented area for 4 classes of age. N= 49. (D) Left: NET1-mCherry (top) and GFP-LacI (bottom) mean nucleolar fluorescence for the same 3 single cells as a function of generation, after SEP alignment. Middle: averaged mean fluorescence of NET1-mCherry (red) and GFP-LacI (green) as a function of generation, after SEP alignment. Right: normalized mean fluorescence of NET1-mCherry (red) and GFP-LacI (green) for 4 classes of age. N= 49 cells.

Figure S2: related to Figure2. (A) Left: pictures of a mother cell with NET1-GFP marker trapped in a cavity in a microfluidic chip. Middle: total NET1-GFP fluorescence averaged after SEP alignment. Right: normalized NET1-GFP fluorescence for 4 classes of age. N= 44 cells. (B) RNA FISH on CHIP for NET1-GFP strain. Same as Fig2C and 2D with a strain containing NET1-GFP marker instead of RPA190-GFP.

Figure S3: related to Figure3. (A) Normalized ratio of NOG2-GFP total fluorescence over cellular area for 4 classes of age. (B) Same as (A) for RPL13A-GFP. (C) Normalized growth rate for 4 classes of age. (D) Same as (A) for RPA190-GFP. (E) Same as (A) for SSF1-GFP. (F) From left to Right: pictures of a mother cell with ACT1pr-NLS-sfGFP, trapped in a cavity, before and after SEP. NLS-sfGFP total fluorescence and N/C ratio (calculated from NLS-sfGFP segmentation) as a function of generation, averaged after SEP alignment. Normalized N/C ratio for 4 classes of mother age. N= 14 cells. (G) Same as (F) for ACT1pr-sfGFP marker instead of ACT1pr-NLS-sfGFP. N= 28 cells. (H) From left to Right: pictures of a mother cell with VPH1-GFP, trapped in a cavity, before and after SEP. VPH1-GFP total fluorescence and vacuolar/cellular ratio as a function of generation after SEP alignment. Normalized vacuolar/cellular ratio for 4 classes of mother age. N= 26 cells. Scale bar: 5µm (for all pictures).

Figure S4: related to Figure5. (A) RPA190-GFP fluorescence in daughter cells for WT (green, N= 21 cells), "fob1 with SEP" (blue, N= 12 cells), "fob1 NO SEP" (magenta, N= 8 cells) after SEP alignment. (B) Cell area in fob1Δ and WT after birth alignment. (C) Cell area in fob1Δ (N= 64 cells) and WT (N= 123 cells) after SEP alignment.

Table1

strain	N	RLS	% NO SEP	RLS NO SEP	RLS with SEP	SEP
BY4742	61	29	7	35	28	20
fob1Delta	126	36	68.25	37	34	30
NET1-GFP	51	19	9.8	14	19	14.5
fob1D+NET1-GFP	135	43	58	48	37	30
RPA190-GFP	78	19	11.5	13	19	14
fob1D+RPA190-GFP	101	34	64.4	39	22.5	21
HTB2-sfGFP	112	27.5	18.75	39	26	19
fob1D+HTB2-sfGFP	56	39	62.5	45	33	27

Material and Methods

Yeast strains, plasmids and media

All strains used in this study are congenic to S288C, except TMY8-BY4B (strain TMY8 back-crossed 4 times with BY4742/41). All GFP-labeled strains were provided from M. Knop GFP collection. Fob1Δ strain was purchased from Euroscarf, crossed with strains containing relevant GFP markers and genotyped by PCR. The HTB2-sfGFP, Act1pr-sfGFP and Act1pr-NLS-GFP strains were generated using DNA editing and yeast genetics techniques.

Prior to loading into microfluidic chips, freshly thawed cells were grown overnight and then diluted in the morning to allow a few divisions in exponential growth.

RNA FISH buffers:
-Buffer B: 54.66g sorbitol + 25ml Phosphate Buffer + 195ml sterile water (250ml final volume)
-Phosphate buffer: 136.09g KH_2PO_4 +228.23g K_2HPO_4 (1L final volume)
-Zymolase mix: 2ml buffer B + 4µL PMSF (stock: 0.1M) + 20µL Vanadium (stock: 200mM) + 4µL βME (stock: 14.3M pur) + 20µL Zymolase 100T (stock 5mg/ml in water)
-20x SSC: 175.3g NaCl + 82.3g Sodium tri Citrate + adjust to 1L with H_2O
-Hybridation mix solution A: 4µl FISH probe (stock 10ng/µl) + 8µl pur formamide + 4µl 2xSSC + 4µl tRNA (stock 10mg/ml) + 14µl H_2O
-Hybridation mix solution B: 2µl BSA (5% in 4xSSC) + 4µl Vanadium (stock: 200mM) + 40µL 4xSSC.
To prepare hybridation mix, solution A was incubated 5min at 98°C then added to solution B at RT.

FISH probe sequence: GCACAGAAATCTCTCACCGTTTGGAATAGCAAGAAAGAAACTTACAAGC with Cy3 dye in 5'. The probe targets ITS1 region between the A2 cleavage site and the 18S coding region.

Microfluidics

The microfluidic master mold was made using standard soft-lithography techniques in the FEMTO-ST nanotechnology platform of the French Renatech network (Besançon, France). Prototypic molds were replicated in epoxy to ensure long-term preservation. The micro-channels were cast by curing PDMS (Sylgard 184, 10:1 mixing ratio) and then covalently bound to a 24 × 50 mm coverslip using plasma surface activation (Diener, Germany). The assembled chip was then baked 1 hour at 60°C to consolidate covalent bonds between glass and PDMS and then perfused with media circulating in Tygon tubing with a peristaltic pump (Ismatec, Switzerland) at a 10µL/min flow rate. After 2 hours of PDMS rehydration, yeast cells were loaded to the chip with a 1ml syringe and a 23G needle.

Time-Lapse Microscopy

All experiments have been replicated at least twice.

Cells were imaged using an inverted Nikon Ti-E microscope. Fluorescence illumination was achieved using LED light (Lumencor) and light was collected using a 60× N.A. 1.4 objective and a CMOS camera Hamamatsu Orca Flash 4.0. We used an automated stage in order to follow up to 60 positions in parallel over the course of the experiment. Images were acquired every 10 or 15 min for a total duration of 140 hours (full lifespan) or 60 hours (RNA FISH) using NIS software. Focus was maintained with the Nikon Perfect Focus System. A constant temperature of 30°C was maintained on the chip using custom sample holder with thermoelectric modules, an objective heater with heating resistors and a PID controller (5C7-195, Oven Industries).

Image Analysis

After acquisition, NIS raw data were analyzed using custom matlab software: phylocell and autotrack available on //github.com/gcharvin. Cell contours and fluorescent markers were segmented using a watershed algorithm and tracking was achieved with the Hungarian method.

RNA FISH on CHIP

Time-lapse was stopped after 60 hours acquisition. 4% paraformaldehyde was perfused in the chip for 30 min at RT for cell fixation then the chip was washed with buffer B for 20min. Cell wall was digested by flowing zymolase mix for 20 min at RT followed by a 20min wash of buffer B. We then rinsed the chip with cold 70% ethanol for 5min, then 15min with 2xSSC, then 20min with 10% formamide in 2xSSC. Hybridation mix with 1ng/µl FISH probe was injected into the chip which was then kept at 37°C for 3hours. After hybridation, we rinsed the chip 30 min with warm (37°C) 10% formamide in 2xSSC, then 20 min with Triton X-100 (1% in 2xSSC) and finally 30min with 1xSSC. Cells in the chip were then imaged on a Nikon Ti-Eclipse with a mCherry filter to acquire FISH probe signal (50% led power, 300ms exposure time, binning 2x2) with a

GFP filter for RPA190-GFP/NET1-GFP signal (20% led power, 100ms exposure time, binning 2x2) and in phase contrast.

Acknowledgements

This work was partly supported by the French RENATECH network. We thank Denis Fumagalli and the MEDIAPREP facility of IGBMC for preparing media. We thank Prof. Takehiko Kobayashi for providing the strain TMY8. We are grateful to Theo Aspert and Sophie Quintin for careful reading of the manuscript.

Author contributions

SM, OG and GC designed the project. SM and SJ carried out research and analyzed data. SM and ILS developed the "FISH on chip" methodology. AM designed the yeast strains used in this study. SM wrote the manuscript.

References

Brewer, B.J., and Fangman, W.L. (1988). A Replication Fork Barrier at the 3 'End of Yeast Ribosomal RNA Genes. Cell *55*, 637-643.

Dammann, R., Lucchini, R., Koller, T., and Sogo, J.M. (1993). Chromatin structures and transcription of rDNA in yeast Saccharomyces cerevisiae. Nucleic Acids Res *21*, 2331-2338.

Defossez, P.-A., Prusty, R., Kaeberlein, M., Lin, S.-J., Ferrigno, P., Silver, P.A., Keil, R.L., and Guarente, L. (1999). Elimination of Replication Block Protein Fob1 Extends the Life Span of Yeast Mother Cells. Molecular Cell *3*, 447-455.

Denoth-Lippuner, A., Krzyzanowski, M.K., Stober, C., and Barral, Y. (2014). Role of SAGA in the asymmetric segregation of DNA circles during yeast ageing. Elife *3*.

Egilmez, N.K., and Jazwinski, S.M. (1989). Evidence for the Involvement of a Cytoplasmic Factor in the Aging of the Yeast Saccharomyces cerevisiae. Journal of Bacteriology *171*, 37-42.

Fehrmann, S., Paoletti, C., Goulev, Y., Ungureanu, A., Aguilaniu, H., and Charvin, G. (2013). Aging yeast cells undergo a sharp entry into senescence unrelated to the loss of mitochondrial membrane potential. Cell Rep *5*, 1589-1599.

Gadal, O., Strauss, D., Petfalski, E., Gleizes, P.E., Gas, N., Tollervey, D., and Hurt, E. (2002). Rlp7p is associated with 60S preribosomes, restricted to the granular component of the nucleolus, and required for pre-rRNA processing. J Cell Biol *157*, 941-951.

Ganley, A.R., Ide, S., Saka, K., and Kobayashi, T. (2009). The effect of replication initiation on gene amplification in the rDNA and its relationship to aging. Mol Cell *35*, 683-693.

Ganley, A.R., and Kobayashi, T. (2014). Ribosomal DNA and cellular senescence: new evidence supporting the connection between rDNA and aging. FEMS Yeast Res *14*, 49-59.

Goulev, Y., Morlot, S., Matifas, A., Huang, B., Molin, M., Toledano, M.B., and Charvin, G. (2017). Nonlinear feedback drives homeostatic plasticity in H2O2 stress response. Elife *6*.

Ide, S., Saka, K., and Kobayashi, T. (2013). Rtt109 prevents hyper-amplification of ribosomal RNA genes through histone modification in budding yeast. PLoS Genet *9*, e1003410.

Janssens, G.E., Meinema, A.C., Gonzalez, J., Wolters, J.C., Schmidt, A., Guryev, V., Bischoff, R., Wit, E.C., Veenhoff, L.M., and Heinemann, M. (2015). Protein biogenesis machinery is a driver of replicative aging in yeast. Elife *4*, e08527.

Jorgensen, P., Edgington, N.P., Schneider, B.L., Rupes, I., Tyers, M., and Futcher, B. (2007). The Size of the Nucleus Increases as Yeast Cells Grow Mol Biol Cell *18*, 3523-3532.

Kennedy, B.K., Austriaco Jr., N.R., and Guarente, L. (1994). Daughter Cells of Saccharomyces cerevisiae from Old Mothers Display a Reduced Life Span The Journal of Cell Biology *127*, 1985-1993.

Kobayashi, T. (2003). The Replication Fork Barrier Site Forms a Unique Structure with Fob1p and Inhibits the Replication Fork. Molecular and Cellular Biology *23*, 9178-9188.

Kobayashi, T. (2008). A new role of the rDNA and nucleolus in the nucleus—rDNA instability maintains genome integrity. BioEssays *30*, 267-272.
Kressler, D., Hurt, E., and Bassler, J. (2017). A Puzzle of Life: Crafting Ribosomal Subunits. Trends Biochem Sci *42*, 640-654.
Kume, K., Cantwell, H., Neumann, F.R., Jones, A.W., Snijders, A.P., and Nurse, P. (2017). A systematic genomic screen implicates nucleocytoplasmic transport and membrane growth in nuclear size control. PLoS Genet *13*, e1006767.
Li, Y., Jin, M., O'Laughlin, R., Bittihn, P., Tsimring, L.S., Pillus, L., Hasty, J., and Hao, N. (2017). Multigenerational silencing dynamics control cell aging. Proc Natl Acad Sci U S A *114*, 11253-11258.
Lu, K.L., Nelson, J.O., Watase, G.J., Warsinger-Pepe, N., and Yamashita, Y.M. (2018). Transgenerational dynamics of rDNA copy number in Drosophila male germline stem cells. Elife *7*.
Mansisidor, A.R., Molinar, T., Srivastava, P., Blitzblau, H., Klein, H., and Hochwagen, A. (2018).
Miyazaki, T., and Kobayashi, T. (2011). Visualization of the dynamic behavior of ribosomal RNA gene repeats in living yeast cells. Genes Cells *16*, 491-502.
Mortimer, R.K., and Johnston, J.R. (1959). Life Span of Individual Yeast Cells. Nature *183*, 1751-1752.
Nakaoka, H., and Wakamoto, Y. (2017). Aging, mortality, and the fast growth trade-off of Schizosaccharomyces pombe. PLoS Biol *15*.
Neumann, F.R., and Nurse, P. (2007). Nuclear size control in fission yeast. J Cell Biol *179*, 593-600.
Nishimura, K., Kumazawa, T., Kuroda, T., Katagiri, N., Tsuchiya, M., Goto, N., Furumai, R., Murayama, A., Yanagisawa, J., and Kimura, K. (2015). Perturbation of ribosome biogenesis drives cells into senescence through 5S RNP-mediated p53 activation. Cell Rep *10*, 1310-1323.
Saka, K., Ide, S., Ganley, A.R., and Kobayashi, T. (2013). Cellular senescence in yeast is regulated by rDNA noncoding transcription. Curr Biol *23*, 1794-1798.
Shcheprova, Z., Baldi, S., Frei, S.B., Gonnet, G., and Barral, Y. (2008). A mechanism for asymmetric segregation of age during yeast budding. Nature *454*, 728-734.
Sinclair, D.A., and Guarente, L. (1997). Extrachromosomal rDNA Circles— A Cause of Aging in Yeast. Cell *91*, 1033-1042.
Spivey, E.C., Jones, S.K., Rybarski, J.R., Saifuddin, F.A., and Finkelstein, I.J. (2017). An aging-independent replicative lifespan in a symmetrically dividing eukaryote. Elife *6*.
Takeuchi, Y., Horiuchi, T., and Kobayashi, T. (2003). Transcription-dependent recombination and the role of fork collision in yeast rDNA. Genes Dev *17*, 1497-1506.
Tiku, V., Jain, C., Raz, Y., Nakamura, S., Heestand, B., Liu, W., Spath, M., Suchiman, H.E.D., Muller, R.U., Slagboom, P.E.*, et al.* (2016). Small nucleoli are a cellular hallmark of longevity. Nat Commun *8*, 16083.

Figure 1

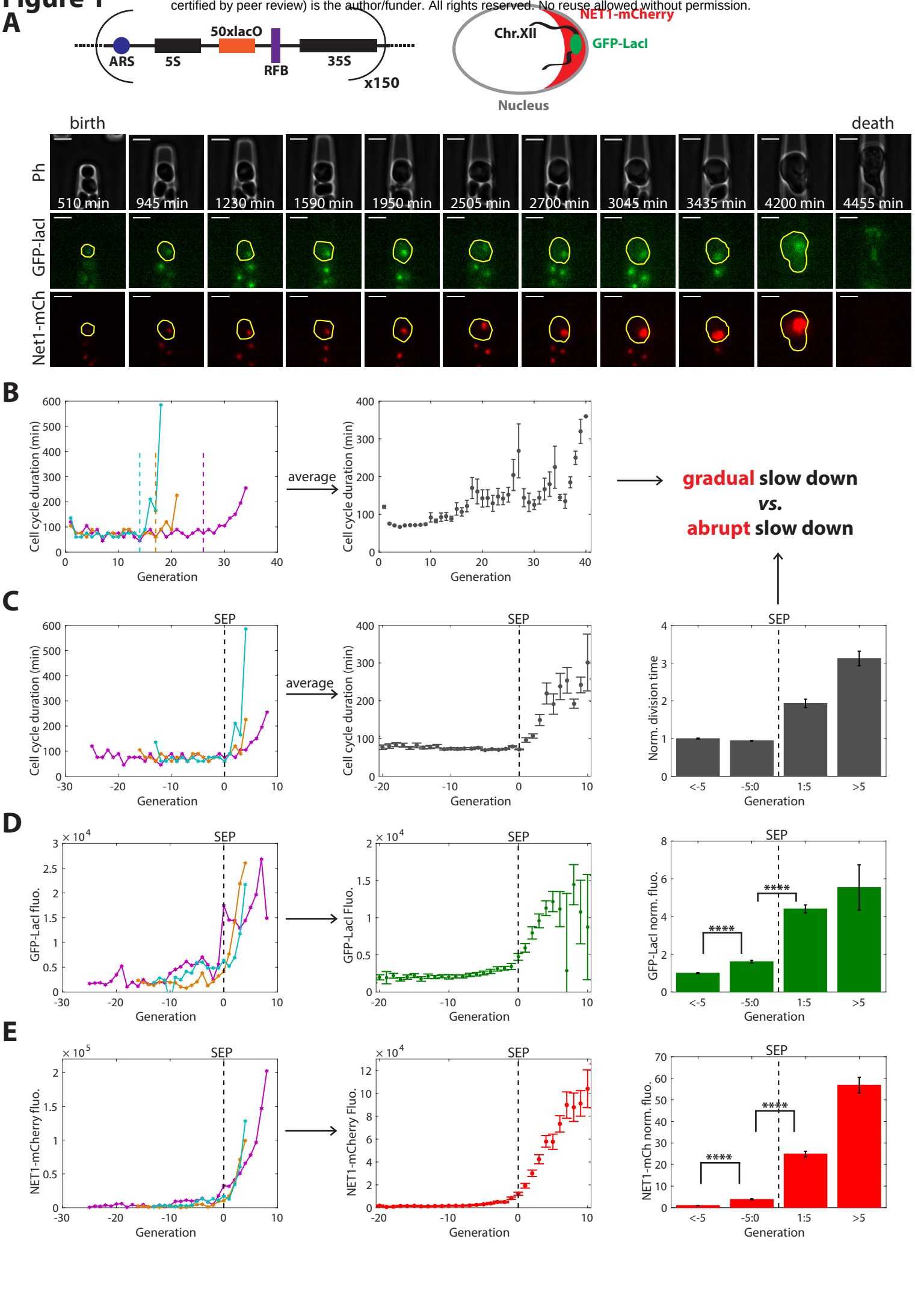

Figure 2

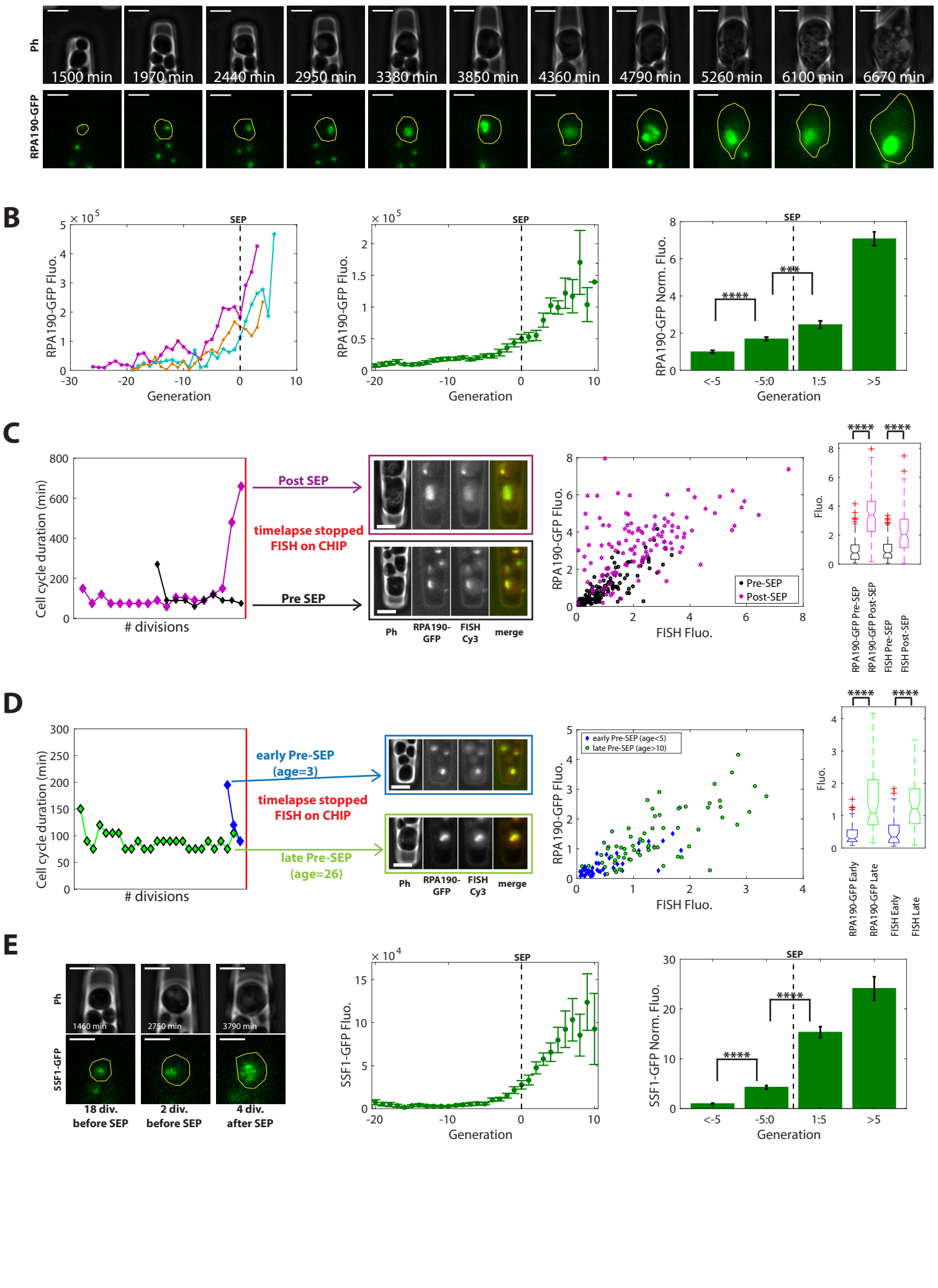

Figure 3

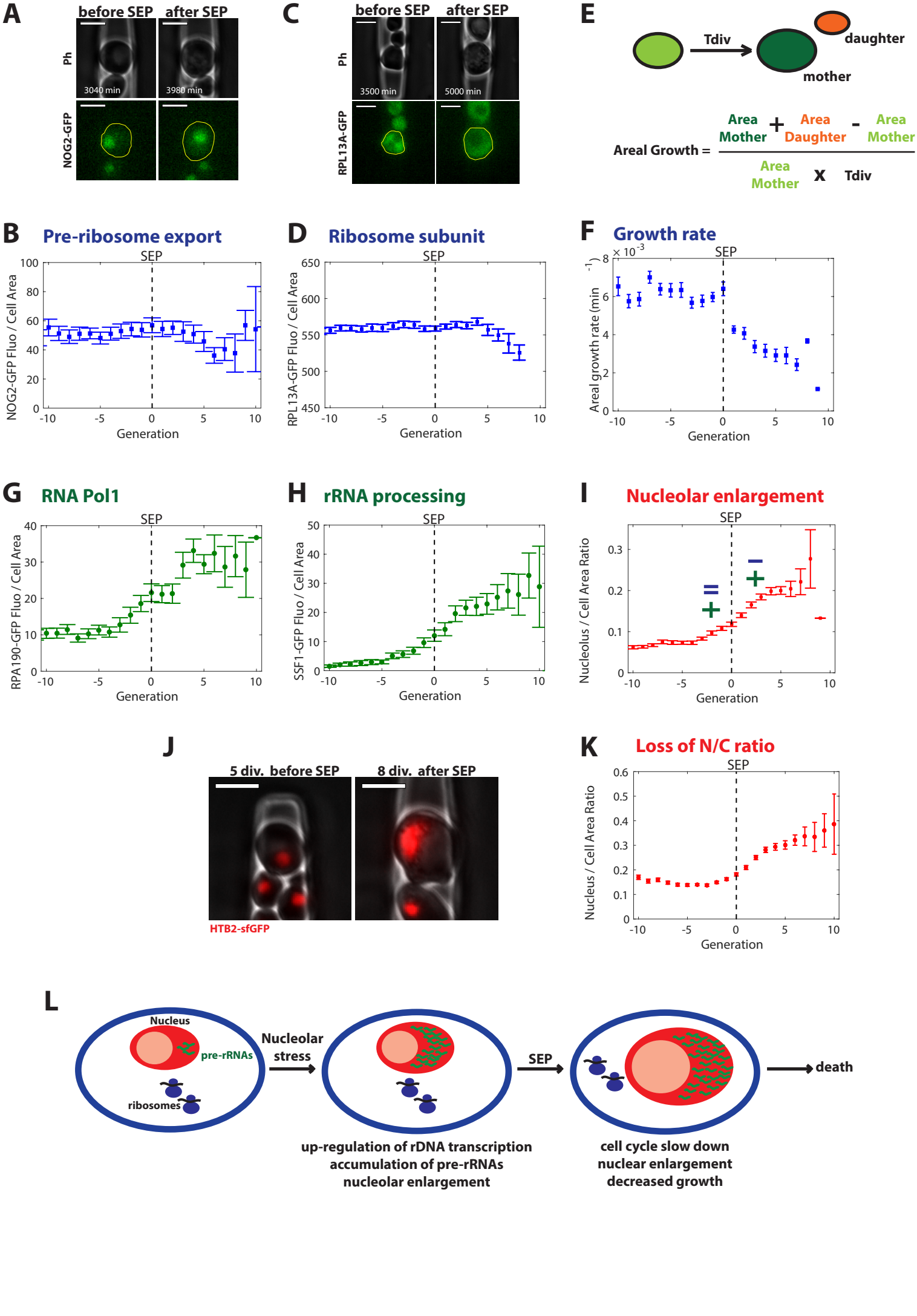

Figure 4

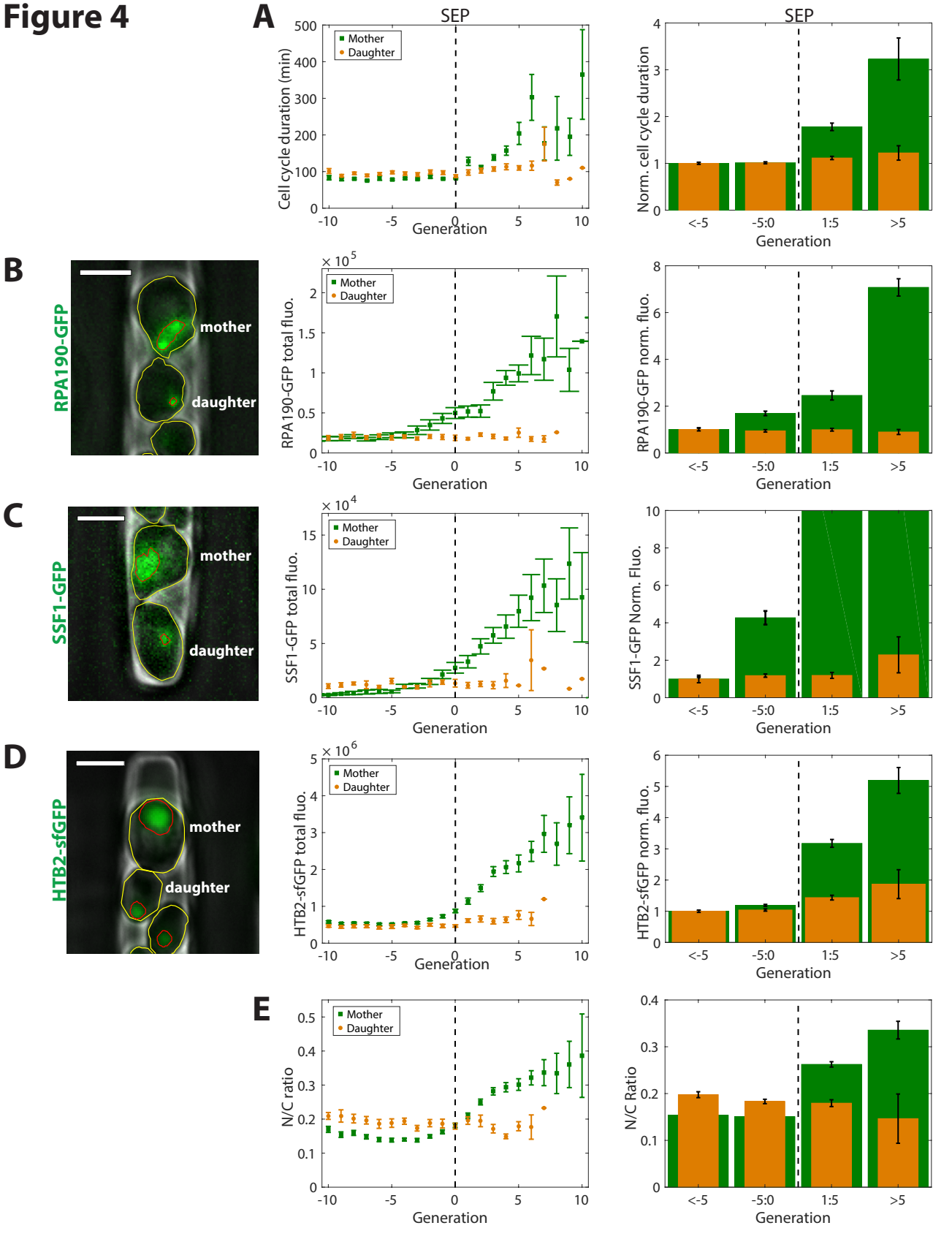

Figure 5

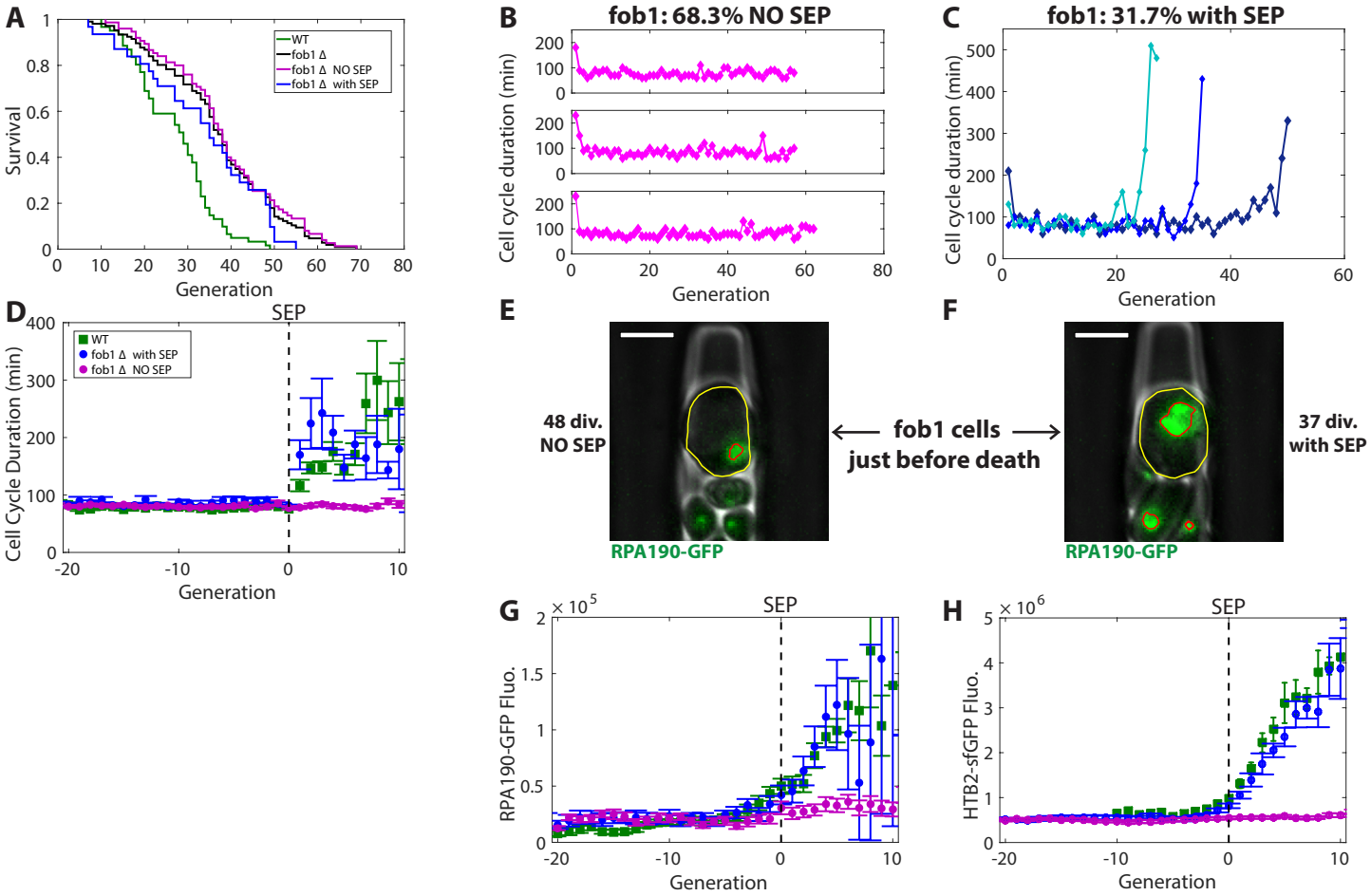

Figure S1

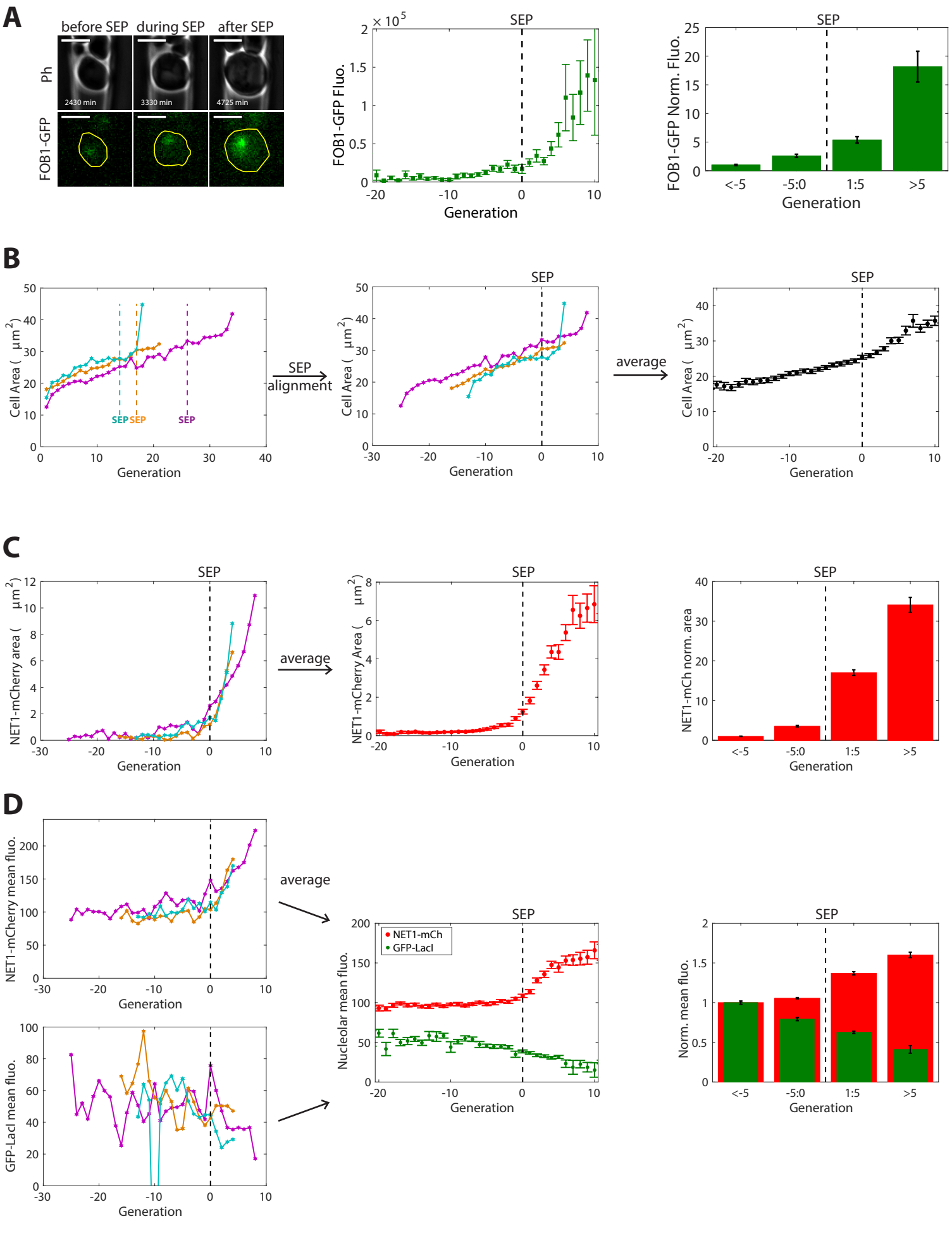

Figure S2

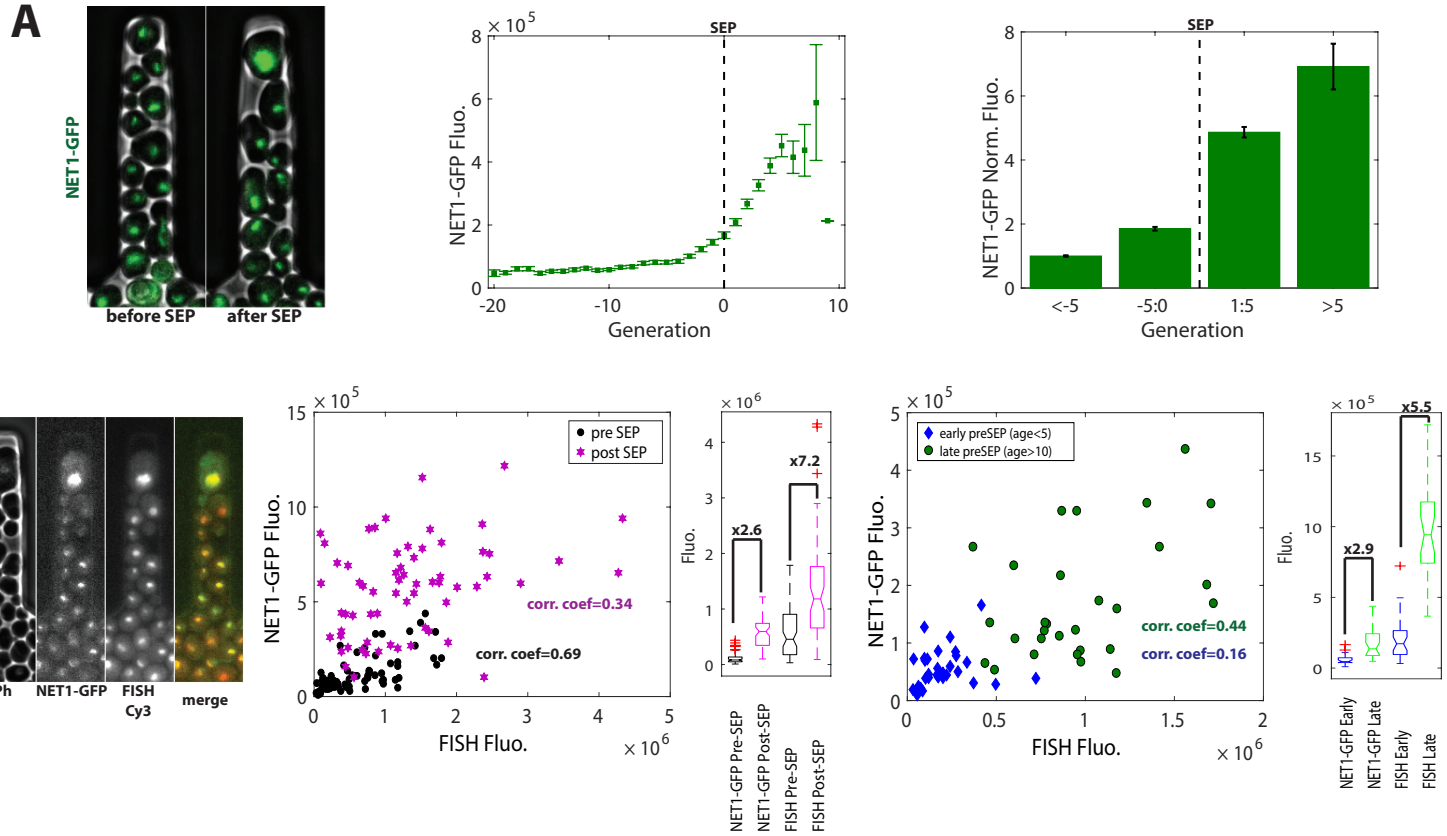

Figure S3

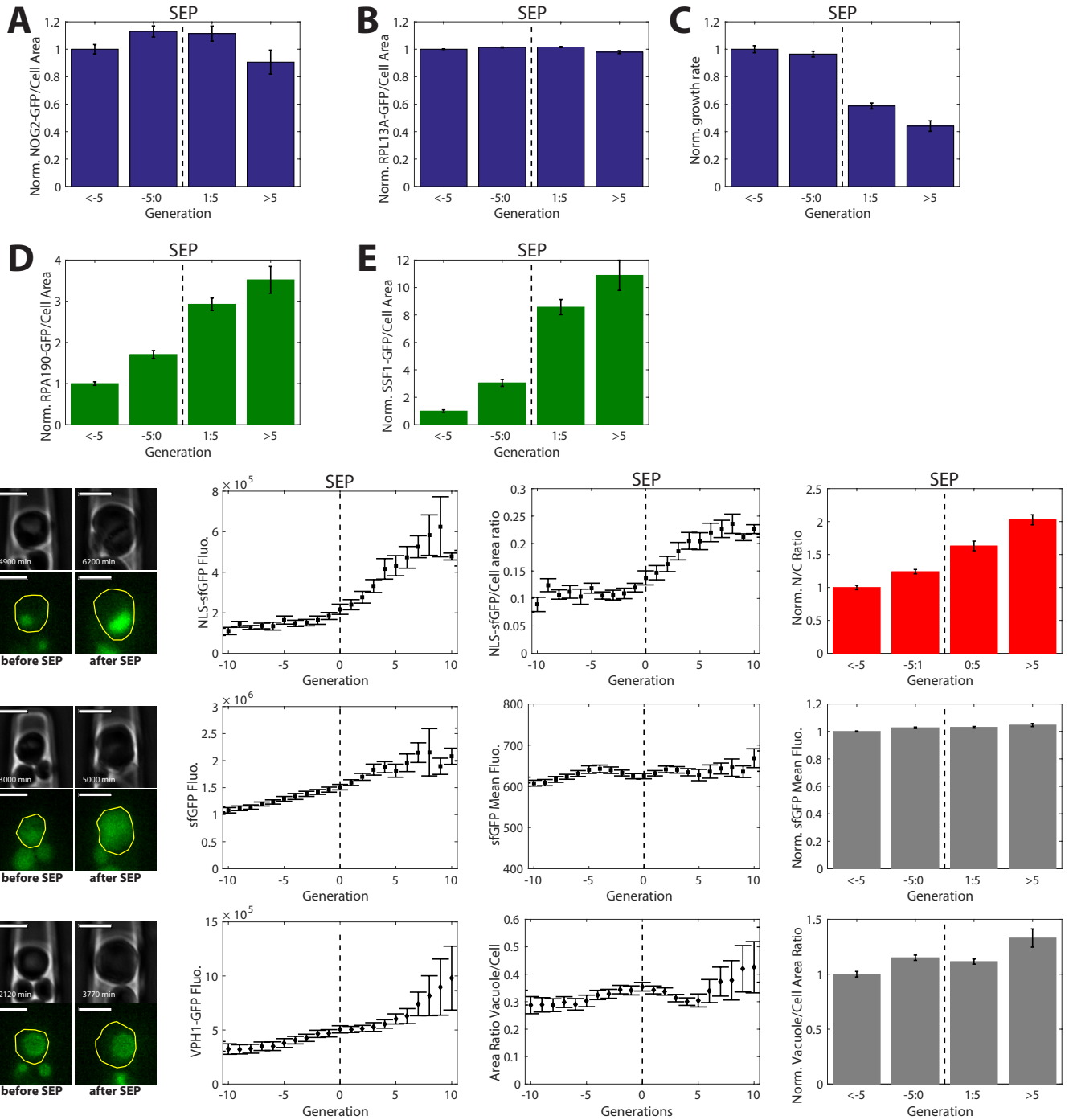

Figure S4